

Avalanche Statistics of Driven Granular Slides in a Miniature Mound

D.E. Juanico

National Institute of Physics, University of the Philippines
1101 Diliman, Quezon City, Philippines

A. Longjas

National Institute of Physics, University of the Philippines
1101 Diliman, Quezon City, Philippines

R. Batac

National Institute of Physics, University of the Philippines
1101 Diliman, Quezon City, Philippines

C. Monterola

National Institute of Physics, University of the Philippines
1101 Diliman, Quezon City, Philippines

We examine avalanche statistics of rain- and vibration-driven granular slides in miniature soil mounds using experimental and numerical approaches. A crossover from power-law to non power-law avalanche-size statistics is demonstrated as a generic driving rate ν is increased, due to diminishing timescale separation ($\sim \nu^{-1}$) between stress buildup and release. For slowly-driven mounds, the tail of the avalanche-size distribution is a power-law with exponent -2.37 ± 0.40 , significantly close to previous findings in empirical landslide data sets. The interevent occurrence time is also analyzed for slowly-driven mounds and it is found that its distribution also follows a power-law trend with exponent ≈ -1.8 .

Landslides are the movement of a mass of rock, debris, or earth down a slope triggered by a variety of natural factors, ranging from rainfall to volcanic activity. The October 2007 landslide that occurred in La Jolla, California, which left almost a hundred casualties and millions of property damages along its wake, is testament of the destructive potential of landslides. The Philippines has had its share of landslide-caused tragedies in densely inhabited mountainous areas. On 17 February 2006, a series of mudslides caused widespread damage and loss of life in Southern Leyte, Philippines. The deadly landslides followed a ten-day period of persistent downpour and a minor ($M2.6$) earthquake.

Spatial prediction of landslide hazards are usually implemented with the guidance of landslide inventory maps [Van Den Eeckhaut et al., 2006]. However, such maps merely pinpoint probable sites of future landslide events (whereby “event” refers to an individual landslide resulting from a trigger) over a particular region on the basis of historical records of past events in that region. Inventory maps do not tell us how large the expected event would be. This prediction uncertainty is addressed by studying the statistics of landslide event sizes, particularly the characterization of empirical frequency-size distributions of landslide scars recorded in historic inventory maps [Guzzetti et al., 2002].

The practical approach to the analysis of underlying physical processes, presumed to generate the statistics of landslide events, is numerical modeling. Contrary to elaborate geophysical landslide susceptibility models, an interesting class of models, based on *self-organized criticality* [Hergarten and Neugebauer, 1998; Piegari et al., 2006] offer simple and insightful elucidation to the possible generating mechanism of avalanche size statistics revealed from large-scale landslide inventory maps. Self-organized criticality, or SOC, is a theory underlying the spontaneous emergence of critical-like behavior (as demonstrated by power-laws and critical exponents) in systems characterized by a separation of timescales between buildup and release of stress, regardless of whether the stress-transfer mechanism is conservative or non-conservative [Juanico et al., 2007a, b; Juanico and Monterola, 2007]. Timescale separation in landslides is exhibited by the fact that it typically takes months or years for a mountain slope to accumulate stress whereas an individual landslide (stress releasing) event itself lasts in a matter of seconds. Timescale separation is intimately connected to the existence of thresholds and metastability [Juanico and Monterola, 2007]. Furthermore, SOC implies a generic triggering mechanism causing the stress buildup, which in this study is interpreted as rainfall, earthquake, or a combination of both.

The present work examines avalanche statistics of rain- and vibration-driven granular slides occurring in miniature soil mounds set up in a laboratory. A previous study [Katz and Aharonov, 2006] explored the generation of a variety of slope-failure types by horizontal and vertical vibrations in a miniature sandbox much like our present experimental setup. It was shown that vertical shaking leads to a power-law distribution of slide-block surface area, although the experiment failed to demonstrate the occurrence of a rollover so prominent in empirical data sets from landslide inventories [Guzzetti et al., 2002; Malamud et al., 2004a, b]. In the present study, we incorporate rainfall as a triggering mechanism and show that its presence allows our model to capture the rollover. Likewise, we demonstrate experimentally the existence of a crossover from power-law to non power-law statistics as theoretically predicted in [Piegari et al., 2006].

The experimental set-up (Figure 1) consists of a soil mound (total mass = 1500g) disturbed by two types of triggering factors: rainfall and vibration. Initially, the mound

is a near-perfect cone in shape (prepared by pouring dry soil onto the platform from a 1-cm funnel hole), and is critically stable such that the slope is at the repose angle (roughly 45° from horizontal; determined experimentally).

Rainfall is simulated using an improvised sprinkler at the top of the mound. Water flows out of the sprinkler through a 3×3 array of circular holes (diameter = 1.0 ± 0.2 mm; center-to-center distance = 5.0 mm). Pour rate is defined as water mass flowing out of the sprinkler per unit time, and the initial water level in the sprinkler controls its value. Data are collected only within the time interval that the pour rate is constant, at the following values: 3.21 g s^{-1} ; 6.60 g s^{-1} ; and 21.09 g s^{-1} .

Horizontal vibrations are applied using a miniature tabletop earthquake simulator. It has been found that with horizontal shaking at low to moderate accelerations, surface grain flows mainly originate from the topmost layer of the slope resulting in the rapid development of failure planes [Katz and Aharonov, 2006]. As shown in Figure 1, a translational-load platform, powered by a servo motor driven by a USB 6009 DAQ driver (National InstrumentsTM), imparts the horizontal vibrations having sawtooth wave profile. The wave profile is fed into the DAQ driver via LabVIEWTM computer interface. The wave is characterized by a maximum amplitude of 1.5 cm (with respect to center) and by frequencies of: 0.2 Hz, 10 Hz, and 89 Hz. Due to the 3D shape of the mound, slope-parallel and slope-normal accelerations are both present during shaking.

The underlying physics of the avalanche statistics of driven granular slides is investigated by performing numerical experiments of a landslide model proposed in [Piegari et al., 2006], defined as follows. A mountain slope is represented as a 2D inclined plane partitioned into a grid (500 cells \times 500 cells). Each cell k is described by a stress parameter θ_k initialized randomly between 0 and 1 from an arbitrarily chosen rectangular distribution (although the distribution used for initial randomization does not affect the long-term behavior of the model [Piegari et al., 2006]). The randomization merely captures the expected heterogeneity of stress values in actual mountain slopes. Stress in the slope builds up over time by means of a localized (i.e., cell scale) driving: $\theta_k(t + \Delta t) = \theta_k(t) + \nu \Delta t$, where ν is the generic driving rate. For simplicity, it is assumed that ν has the same value for all cells. When a cell k has $\theta_k > 1$, it collapses and transfers all stress to its four nearest neighbors $nn = \{up, down, right, left\}$ at different proportions g_{nn} . By virtue of gravity, stress transfer is biased downwards, such that: $g_{down} > g_{up}$, subject to the constraint $g_{down} + g_{up} = 0.5$; and $g_{left} = g_{right} = 0.25$. In this study, it is assumed that transfer is conservative, so that $\sum_{nn} g_{nn} = 1$. Stress-transfer proceeds until the entire grid relaxes such that all cells have $\theta_k < 1$. All consecutive stress-transfers comprise a landslide event at time t , and the total number of collapsing cells at time t is the landslide area $A(t)$. For correspondence with experiments, we assume a landslide mass-area relation: $M \sim A^{3/2}$.

The novelty in our modeling approach is in considering the observed fact that the slope flattens out eventually after several landslide events have occurred. Thus, an update rule is imposed to decrease g_{down} , as follows: $g_{down}(t + \Delta t) = g_{down}(t) - 10^{-5}A(t)$. The value of g_{up} is updated accordingly via the constraint $g_{down} + g_{up} = 0.5$. This modification incorporates the dynamics of slope evolution which was not realized in [Piegari et al., 2006]. The

generic driving rate ν defined in the model corresponds to the experimental parameters, as shown in Table 1.

Table 1. Correspondence of generic driving rate defined in the model and the experimental parameters. Notice that there are two slow driving rates for the same pour rate. This is based from the observation that at slow pour rates, the avalanche statistics is sensitive to the vibration frequency. However, for moderate and high pour rates, the statistics is no longer sensitive to variations in the vibration frequency within the range 0.2 to 89 Hz.

Description	Driving rate ν	Pour rate (g s^{-1})	Vibration frequency (Hz)
Slow	7.50×10^{-5}	3.21	0.2
Slow	5.00×10^{-5}	3.21	89
Moderate	1.25×10^{-4}	6.60	0.2, 10, 89
Fast	7.50×10^{-4}	21.09	0.2, 10, 89

Avalanche size is interpreted as the mass M of soil falling from the mound onto the basin within a 50-ms interval (approximate temporal resolution of our setup). M is measured by a weighing scale (resolution: 0.1g) beneath the basin, as illustrated in Figure 1. The total sampling period varies with the pour rate. For slow pour rate, ten 10-s samples were made. For moderate pour rate, ten 5-s samples were made and three 3-s samples were done for fast pour rate. These are based on the fact that the slower the pour rate the longer it takes for the entire mound to wash out.

Figure 2 illustrates the normalized histograms of avalanche size resulting from slow (\diamond), moderate (\circ), and fast (\square) driving (as defined in Table 1). Timescale separation is proportional to ν^{-1} ; hence, the observed crossover from power-law to non power-law statistics is attributed to the diminishing timescale separation. The crossover has already been previously recognized in [Piegari et al., 2006]. Rescaled probability mass functions (pmf) resulting from numerical experiments are superimposed over the corresponding experimental histograms, confirming the crossover behavior. Furthermore, the presence of a rollover (inflection) in both experimental and computational data supports the claim that the rollover seen in landslide inventory data sets is not a mere artifact of the limited mapping resolution [Guzzetti et al., 2002; Malamud et al., 2004a, b].

It is expected from the model that as $\nu \rightarrow 0$ (infinite timescale separation limit), the rollover should disappear leaving a pure power-law distribution, in accordance with the Olami-Feder-Christensen model [Olami et al., 1992]—the limiting case of our model as $\nu \rightarrow 0$. The tail of the pmf resulting from our model for a slowly-driven ($\nu \approx 0$) mound yields a power-law exponent -2.37 ± 0.40 , which is significantly close to -2.40 (two-tailed t-test: $t = 0.71$, $df = 85$, $p = 0.48$) determined by previous studies [Malamud et al., 2004a, b]. To the extent that our experiment and numerical results agree, we attribute the rollover to the finiteness, albeit small, value of the driving rate ν characterizing real systems. This rollover becomes more pronounced, such that the peak shifts towards larger avalanche sizes, as ν increases. At $\nu \sim 10^{-4}$, the avalanche size distribution appears more like a normal (or Gaussian) distribution. Thus, ν guides the crossover from power-law to non power-law statistics. An implication of this crossover is that under high-rate driving (especially by frequent rainfall), the landslide behavior of mountain slopes appears to collapse to a state wherein a large avalanche size is almost always expected. It is thus not surprising that rain-induced landslides more often occur in areas frequently struck by storms (e.g., Southern Leyte,

Philippines). However, a more comprehensive description of ν should incorporate ground-failure factors such as soil composition. Such factors have been neglected in this study for simplicity.

A relevant aspect for hazard prediction is the interevent occurrence time statistics. The interevent occurrence time is the interval between the peaks of events whose sizes are above the threshold ($M = 0.8$ g), which corresponds approximately to the peak of the pmf (\diamond , Figure 2). We thus gathered time series of avalanche size $M(t)$ in slowly-driven mounds over a period of 20 s. Figure 3 illustrates a representative sample for the first 10 s of this time series for both experiment and computational data. A thresholding procedure is applied to discard events whose sizes are below the threshold. The region $M < 0.8$ g corresponds to the rollover portion of the pmf (\diamond , Figure 2) for slowly-driven mounds. The vertical demarcation line in Figure 2 corresponds to horizontal demarcation line in Figure 3. The pmf for interevent occurrence time derived from experiment and model are shown on the inset graph of Figure 3, and both exhibit power-law trends with exponents -1.812 ± 0.055 (reduced $\chi^2 = 7.88 \times 10^{-5}$, $df = 88$) and -1.806 ± 0.021 (reduced $\chi^2 = 1.21 \times 10^{-5}$, $df = 35$), respectively.

Power-law interevent occurrence time distribution implies that most correlated events are clustered in time, which seems to agree with recent findings [Rossi *et al.*, 2007, 2008]. The power-law trend further implies that correlated events may be separated a long time from each other—a landslide event today may be linked with an earlier event a long time ago. This may be the reason that in landslide inventories, newer landslide scars are typically situated at or near areas where older scars exist. The long temporal correlation, which a power-law interevent time distribution appears to suggest, could possibly be due to rainfall seasonal trends [Rossi *et al.*, 2008].

The general agreement of our results with empirical data suggests that miniature experimental models may suffice in understanding several underlying facets of complex landslide processes (statistical properties, self-organization). While several factors that others may argue as necessary are neglected in describing the system, such as soil porosity, rock type, pore-water pressure, humidity and other geophysical parameters, the SOC landslide model presented here delivers basic insights that would guide more detailed explorations later on.

Acknowledgments.

The authors acknowledge the reviewers for their valuable comments that remarkably improved the presentation quality of this manuscript. We also thank Engr. Bernardino Buenaobra for assistance on instrumentation; Engrs. Osmonn Burgos and Mike Abundo for providing the earthquake simulator; and funding from the UP-OVPAA (C.M.), UP-OVCRD (D.E.J.), and DOST (A.L. and R.B.).

References

- Guzzetti, F., B. Malamud, D. Turcotte, and P. Reichenbach (2002), Power-law correlations of landslide areas in central Italy, *Earth Planet. Sci. Lett.*, *195*, 169.
- Hergarten, S. and H. Neugebauer (1998), Self-organized criticality in a landslide model, *Geophys. Res. Lett.*, *25*, 2382.
- Juanico, D.E., C. Monterola, and C. Saloma (2007a), Self-organized critical branching in systems that violate conservation laws, *New J. Phys.*, *9*, 92.
- Juanico, D.E., C. Monterola, and C. Saloma (2007b), Dissipative self-organized branching in a dynamic population, *Phys. Rev. E*, *75*, 045105R.
- Juanico, D.E. and C. Monterola (2007), Background activity drives criticality of neuronal avalanches, *J. Phys. A*, *40*, 9297.
- Katz, O. and E. Aharonov (2006), Landslides in a vibrating sand box: What controls types of slope failure and frequency magnitude relations?, *Earth Planet. Sci.*, *247*, 280.

Malamud, B., D. Turcotte, F. Guzzetti and P. Reichenbach (2004a), Landslide inventories and their statistical properties, *Earth Surf. Process. Land.*, *29*, 687.

Malamud, B., D. Turcotte, F. Guzzetti and P. Reichenbach (2004b), Landslide, earthquakes, and erosion, *Earth Planet. Sci. Lett.*, *229*, 45.

Olami, Z., H.J.S. Feder and K. Christensen (1992), Self-organized criticality in a continuous nonconservative cellular automaton modeling earthquakes, *Phys. Rev. Lett.*, *68*, 1244.

Piegari, E., V. Cataudella, R. Di Maio, L. Milano and M. Nicodemi (2006), A cellular automaton for the factor of safety field in landslides modeling, *Geophys. Res. Lett.*, *33*, L01403.

Rossi, M., S. Peruccacci, A. Witt, B.D. Malamud and F. Guzzetti (2008), Characteristics of an historical landslide catalogue for the Emilia-Romagna Region, Northern Italy: frequency-size, temporal clustering and triggering factors, *Geophys. Res. Abs.*, *10*, EGU2008-A-07210.

Rossi, M., S. Peruccacci, A. Witt, F. Guzzetti, B.D. Malamud and M. Pizzoli (2007), Statistical and temporal properties of 596 triggered landslide events in the Emilia-Romagna region of Italy, *Geophys. Res. Abs.*, *9*, 03455.

Van Den Eeckhaut, M., T. Vanwalleghe, J. Poesen, G. Govers, G. Verstraeten and L. Vandekerckhove (2006), Prediction of landslide susceptibility using rare events logistic regression: A case-study in the Flemish Ardennes (Belgium), *Geomorphology*, *76*, 392.

cmonterola@nip.upd.edu.ph, cmonterola@gmail.com

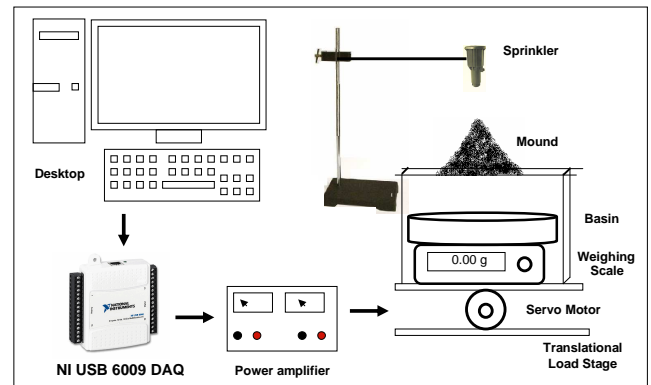


Figure 1. The experimental setup consists of a soil mound (total mass of 1500 g) with initial near-perfect cone shape. Rainfall is simulated by a sprinkler on top of the mound, consisting of an array of holes. Water level inside the sprinkler controls the pour rates at: 3.21, 6.60, and 21.09 g s⁻¹. Earthquake is simulated by a translational load stage that imparts horizontal vibrations to the platform where the mound is placed. The vibrations have a sawtooth wave profile of maximum amplitude of 1.5 cm and frequencies of 0.2, 10, and 89 Hz. The wave profile is encoded by a desktop PC connected via an interface to a DAQ driver. Different parameter combinations are listed on Table 1. Avalanche size is the mass M of soil falling from the mound to the basin within ≈ 50 -ms intervals. Mass is measured by a weighing scale (resolution, 0.1 g) connected to the PC where the readings are registered.

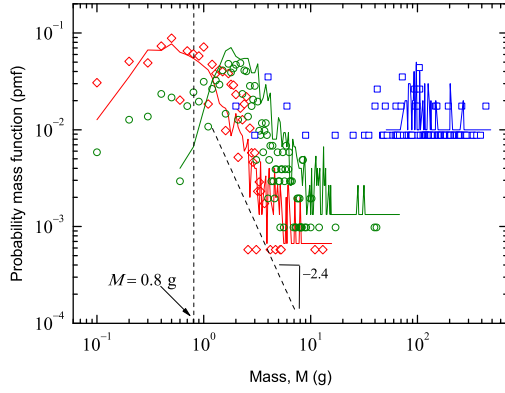


Figure 2. (Color online). Normalized histograms of avalanche size resulting from slow (\diamond), moderate (\circ), and fast (\square) driving. Corresponding pmfs of avalanche size derived from numerical simulations are superimposed after rescaling landslide area into landslide mass using a mass-area relation: $M = (1.0 \times 10^{-5} \text{ g} \cdot \text{cell}^{-3/2}) A^{3/2}$. The tail of the pmf ($M > 0.8 \text{ g}$) for a slowly-driven mound fits a power-law with exponent -2.37 ± 0.40 , significantly close to -2.40 reported in [Malamud *et al.*, 2004a, b]. For moderately-driven mounds, the rollover region of the pmf becomes more extensive as the peak shifts to larger M -values. For highly-driven mounds, the pmf resembles a normal (or Gaussian) distribution centered at a large value of M .

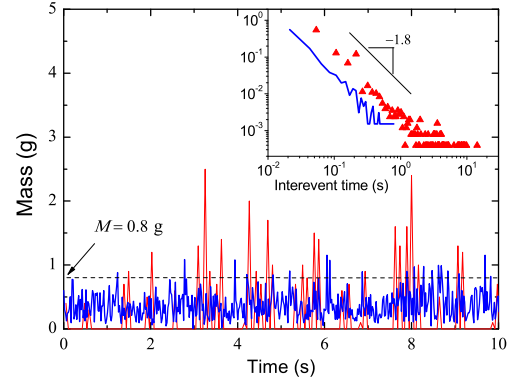


Figure 3. (Color online). Interevent occurrence times. Time series of avalanche size from experiment (red, solid curve) and model (blue, thick curve). Iteration steps (iter) in the model have been rescaled to time (s) using the scaling factor: $0.021254 \text{ s} \cdot \text{iter}^{-1}$. Avalanche area $A(t)$ in the model have also been rescaled into avalanche mass $M(t)$, using $M = (1.0 \times 10^{-5} \text{ g} \cdot \text{cell}^{-3/2}) A^{3/2}$. Avalanche sizes less than 0.8 g are discarded. Interevent occurrence time is the interval between consecutive peaks above the threshold. *Inset:* Interevent time distributions for experiment (red, \blacktriangle) and model (blue, thick curve), both obeying a power-law with exponent -1.812 ± 0.055 and -1.806 ± 0.021 , respectively.